A density functional study of the structural, elastic, optical and thermal properties of the AgAlTe$_2$ under pressure

SHUN-RU ZHANG[a,*], SHUANG-JIAN WANG[a], YUE-BING ZHOU[a], LING-XIA ZHANG[a], LIN-HUA XIE[b]
[a]Department of Physics and Information Engineering, Huaihua University, Hunan 418008, China
[b]Institute of Solid State Physics & School of Physics and Electronic Engineering, Sichuan Normal University, Chengdu 610066, China

First principles density functional theory (DFT) calculations for structural, elastic and optical properties of AgAlTe$_2$ was performed with the local density approximation functional. We found that the obtained lattice constants of AgAlTe$_2$ are in agreement with the available experimental data and other theoretical ones. The elastic constants C_{ij}, bulk modulus B, shear modulus G, Young's modulus E and Debye temperature θ of AgAlTe$_2$ are also presented. In addition, the optical properties such as the dielectric function, refractive index and reflectivity under pressure were also computed and discussed systematically for the first time. Finally, the thermal properties such as thermal expansion, heat capacity, Debye temperature were computed applying the quasi-harmonic Debye model at different temperatures (0-900 K) and pressures (0-2 GPa).

1. Introduction

Over the past few years, ternary chalcopyrite semiconducting compounds I-III-VI$_2$ and I-IV-VI$_2$ have been gaining a considerable attention due to their applications in photocatalytic, photoelectrochemical (PEC) water splitting, optoelectronic and nonlinear optical (NLO) devices [1-7]. From the experimental point of view, AgAlX$_2$(X = S, Se, Te) chalcopyrites have been widely investigated and found to be direct bandgap semiconductors. Generally, the studies on AgAlX$_2$ (X = S, Se, Te) chalcopyrite compounds for PEC systems have mainly focused on sulfides and selelides. However, tellurides with a suitable band gap like CuAlTe$_2$ (2.06 eV) and AgAlTe$_2$ (2.27 eV) have rarely reported as semiconductor photocathodes [8]. In early work, Honeyman et al. have grew single crystals of CuGaS$_2$, CuAlTe$_2$, AgGaS$_2$, AgAlS$_2$ and AgAlSe$_2$ by iodine vapour transport to measure the gap and the refractive index of these compounds [9]. In terms of theoretical investigations, Mishra et. al. have investigated the structural and electronic properties of AgAlX$_2$ (X = S, Se, Te) chalcopyrites using the local density approximation (LDA) for exchange-correlation and a tight-binding linear muffin tin orbital (TB-LMTO) method [10]. Saeed Ullah et. al. have obtained the structural, electronic and optical properties of the ternary semiconducting compounds AgXY$_2$(X = Al, Ga, In and Y = S, Se, Te) in Heusler and chalcopyrite crystal phases using the density functional theory (DFT) based on the full potential linear augmented plane wave (FP-LAPW) method [11]. However, many previous studies demonstrated that the pressures have profound effects on the structural, mechanical, electronic in chalcopyrite semiconducting compounds [12, 13]. The effects of pressure on the mechanical and optical properties have not been calculated or measured in AgAlTe$_2$. In our calculations, we present a detailed investigation on the structural, mechanical, electronic and optical properties of AgAlTe$_2$ by using the first-principles calculation based on density functional theory.

2. Computational details

In this study, we employed the Vanderbilt-type ultrasoft pseudopotential [14] for the interaction between the electrons and the ion cores. The LDA proposed by Vosko et. al. [15] were adopted as the exchange-correlation functional. The details of the parameters are: the electronic wave functions were expanded in a plane wave basis set with the energy cut-off of 550 eV for LDA. For the Brillouin-zone sampling, a 7×7×7 Monkhorst-Pack mesh was used for LDA. The self-consistent convergence of the total energy is 3.0×10^{-5} eV/atom, the maximum ionic Hellmann-Feynman force is 0.05 eV/Å the maximum ionic displacement is 0.004 Å, and the maximum stress is 0.03 GPa. It is found that these parameters are sufficient to lead to desirable results for the studied properties. All these electronic structure calculations are implemented through the CASTEP code [16, 17].

3. Results and discussions

3.1. Ground state structures of AgAlTe$_2$

The ternary semiconductor crystallizes in the chalcopyrite structure with space group I-42d. The Ag atoms are located at (0,0,0); (0,1/2,1/4), the Al atom at (1/2,1/2,0); (1/2,0,1/4) and Te at (u,1/4,1/8); (u,3/4,1/8); (3/4,u,7/8); (1/4,u,7/ 8), where u = 0.260 for AgAlTe$_2$. In Table 1, we list our results together with the available experimental data and other theoretical results. The lattice parameters (a, c) for the AgAlTe$_2$ from LDA, calculations are 6.1947Å and 12.0462Å, respectively. All these results show that the results obtained from LDA calculation are in agreement with the experimental data [19, 20] and other theoretical values [10, 11, 18]. Thus, in the following, we only focus on the results from the LDA calculations.

Table 1. Calculated lattice parameters a and c (Å) for investigated AgAlTe$_2$, compared to available experimental and theoretical values

	This work	Other theoretical calculations			Experiments	
a	6.1947	6.40[a]	6.151[b]	6.22[c]	6.296[d]	6.29[e]
c	12.0462	12.224[a]	11.982[b]	12.2783[c]	11.83[d]	11.8252[e]

[a] Ref.[18]. [b]Ref.[11]. [c]Ref.[10]. [d]Ref. [19]. [e]Ref.[20].

3.2. Elastic properties

The mechanical stability conditions for the tetragonal structures can be expressed in terms of elastic constants [21]

$$C_{11}, C_{33}, C_{44}, C_{66} > 0, \ C_{11} > |C_{12}|, C_{11}C_{33} > C_{13}^2, \text{ and}$$

$$(C_{11} + C_{12})C_{33} > 2C_{13}^2 \tag{1}$$

The pressure dependence of elastic constants are calculated for the first time and given in Table 2, for AgAlTe$_2$. It can be seen that the elastic constants of the AgAlTe$_2$ meet all of these conditions above when the pressure P is below 2 GPa, indicating that the AgAlTe$_2$ is mechanically stable below this pressure. It is found that the elastic constants obtained by LDA method are in favorable agreement with other theoretical data [22]. C_{11}, C_{12}, C_{13} and C_{33} increases under the effect of pressure while C_{44} and C_{66} decreases with pressure.

Table 2. Calculated elastic constants C$_{ij}$(GPa) of AgAlTe$_2$ under 0 pressure up to 2 GPa, together with other theoretical results

Pressure		C_{11}	C_{12}	C_{13}	C_{33}	C_{44}	C_{66}
0	Present	74.75	47.30	47.90	70.27	30.02	28.82
0	Ref[22]	79.90	49.9	58.4	92.20	33.8	30.7
0.5		77.00	49.76	50.35	72.17	29.82	32.32
1		79.26	52.28	52.84	74.31	28.77	29.29
1.5		81.41	54.70	55.22	76.28	28.24	28.19
2.0		83.50	57.14	57.69	78.27	27.34	28.01

Table 3. Calculated bulk modulus B (GPa), shear modulus G (GPa), Young's modulus E(GPa) and Debye temperature θ (K) of AgAlTe$_2$

Pressure	B	G	E	B/G	θ
0	56.19	21.10	56.26	2.66	211.1
	49.83[a]				214.4[b]

[a] Ref. [18]. [b]Ref. [28]

Using the Voigt-Reuss-Hill approximation [23], the calculated bulk modulus B and shear modulus G for AgAlTe$_2$ are 56.19 and 21.10 GPa, respectively. The bulk modulus B obtained by LDA method is 56.19 GPa, which agrees with the data 49.83 GPa obtained by Perdew-Burke-Ernzerhof (PBE) [18]. In addition, Pugh has proposed that a high (low) B/G value, which separates ductile and brittle materials, is about 1.75 [24]. In our work, the B/G of AgAlTe$_2$ is 2.66 at 0 K and 0 GPa, indicating that AgAlTe$_2$ is ductile.

The velocities of the longitudinal (V_l) and transverse (V_t) acoustic wave, and the average acoustic velocity (V_m) can be calculated by [25]

$$V_l = \sqrt{(B + \frac{4}{3}G)\frac{1}{\rho}} \ ,$$

$$V_t = \sqrt{\frac{G}{\rho}} \ , \ V_m = [\frac{1}{3}(\frac{2}{V_t^3} + \frac{1}{V_l^3})]^{-1/3} \qquad (2)$$

Finally, the Debye temperature (θ) can be derived via [26]

$$\theta = \frac{h}{k}[\frac{3n}{4\pi}(\frac{N_A \rho}{M})]^{1/3}V_m \qquad (3)$$

where h is the Planck constant, respectively, N_A is the Avogadro number, M is the molecular weight and ρ is the density.

For AgAlTe$_2$, the calculated Debye temperature θ from elastic constants is 211.1 K, which is well consistent with other calculation for 214.4 K [27]. It is further proved that our elastic constants of AgAlTe$_2$ from LDA calculation is reliable.

3.3. Electronic properties

Using the LDA optimised structural parameters, a systematic study of the band structure and density of states (DOS) were carried out using the LDA functional. The calculated band structure at 0 GPa is given in Fig. 1. The position of the Fermi level is at 0 eV. LDA yields direct bandgap at the Γ point of 1.184 eV for AgAlTe$_2$. The bandgap is in the same range as the previous theoretical results [18], but underestimate the experimental bandgap as expected.
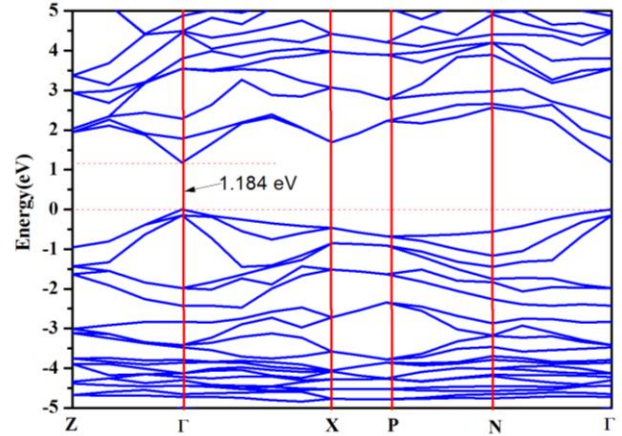
Fig. 1. Band structure of AgAlTe$_2$

The total and partial density of states (DOS and PDOS)) are also indicated in Fig. 2. The partial density of state are very useful as they give information on hybridization and the orbital character of the states. From the partial density of state, we are able to identify the angular momentum character of the different structure. It can be seen that in Fig. 2, the lowest valence bands are essentially dominated by Te-s states, with minor presence Al-p and Al-s states. The intermediate valence band is essentially dominated by Ag-d states. The other valence bands are dominated by Te-p states. The conduction band consists of Te-s and Te-p with a minor presence Al-p and Al-s states. The appearing of the energy gap in DOS confirms the semiconductor nature of AgAlTe$_2$.
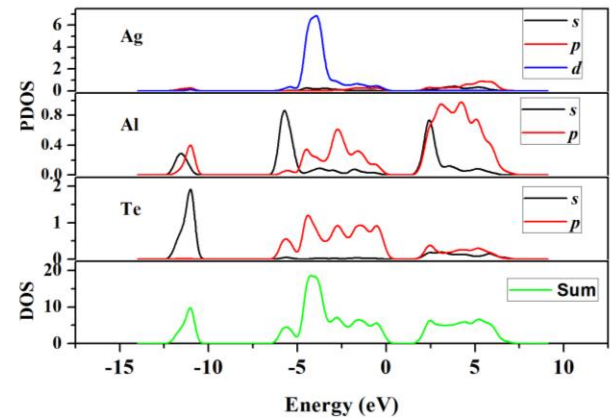
Fig. 2. Total and partial density of state (unit/(states/eV-unit cell)) of AgAlTe$_2$

3.4. The effect of pressure on the optical properties

Optical properties of the crystals are described in terms of the complex dielectric function $\varepsilon(\omega) = \varepsilon_1(\omega) + i\varepsilon_2(\omega)$. The imaginary part $\varepsilon_2(\omega)$ was obtained from the momentum matrix

elements between the occupied and unoccupied wave functions within the selection rules. The real part $\varepsilon_1(\omega)$ of the dielectric function was calculated by the Kramers-Kronig transformation [28] of the imaginary part $\varepsilon_2(\omega)$. Other optical constants were calculated from the values of $\varepsilon_1(\omega)$. For the chalcopyrite structure, the dielectric functions are resolved into two components $\varepsilon_{1xy}(\omega)$ and $\varepsilon_{2xy}(\omega)$ which is the average of the spectra for polarizations along the x and y directions (E $\perp$ c-axis), $\varepsilon_{1z}(\omega)$ and $\varepsilon_{2z}(\omega)$ corresponding to the z direction (E//c-axis). We present the average function of the calculated real and imaginary parts of the dielectric function $\varepsilon_1(\omega) = (\varepsilon_{1x}(\omega) + \varepsilon_{1y}(\omega) + \varepsilon_{1z}(\omega))/3$ and $\varepsilon_2(\omega) = (\varepsilon_{2x}(\omega) + \varepsilon_{2y}(\omega) + \varepsilon_{2z}(\omega))/3$. We also present the average function of the calculated refractive index and reflectivity spectrum in this work.

The obtained real part of dielectric function $\varepsilon_1(\omega)$ are plotted in Fig. 3. The main peaks of the $\varepsilon_1(\omega)$ for AgAlTe$_2$ occur at 2.03, 2.11 and 2.18 eV at 0, 1 and 2 GPa pressures, respectively. An important quantity of $\varepsilon_1(\omega)$ is the zero

frequency limit $\varepsilon_1(0)$. Dielectric constant $\varepsilon_1(0)$ are found to be 9.40, 9.34 and 9.32 eV at 0, 1 and 2 GPa pressures, respectively (see Table 4). When the applied pressure is up to 2 GPa, the peaks in the $\varepsilon_1(\omega)$ increase and shift to the right with a small extend.
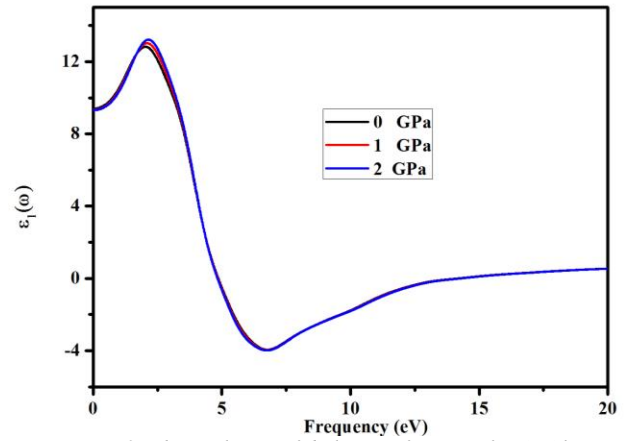
Fig. 3. The real part of dielectric function for AgAlTe$_2$

Table 4. The values of the real dielectric constant $\varepsilon_1(0)$ and refractive index $n(0)$ at different pressures for AgAlTe$_2$

		0	1.0	2.0
$\varepsilon_1(0)$	This work	9.40	9.34	9.32
	Other calculations	9.21[a]		
$n(0)$	This work	3.07	3.06	3.05
	Other calculations	2.62[a] 3.03[a] 2.168[b]		

[a] Ref. [18]. [b] Ref. [29].
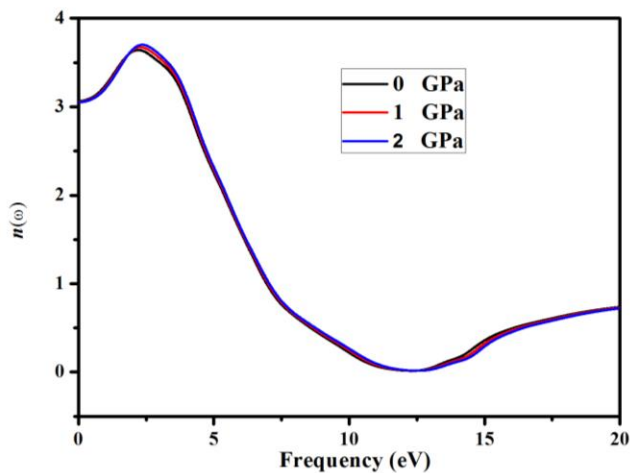
Fig. 4. Refractive index n(ω) for AgAlTe$_2$

The refractive index of a material is very useful optical parameter to determine the propagation of light through the optical medium. The refractive index at 0, 1 and 2 GPa pressures for AgAlTe$_2$ are plotted in Fig. 4. Refractive index increases with energy increases, reaching a maximum value 3.64 at about 2.21 eV for 0 GPa, 3.67 at about 2.29 eV for 1 GPa and 3.70 at about 2.36 eV for 2 GPa. It then decreases to a minimum level at 12.29 eV at 0 GPa, 12.41 at 1 GPa and 12.52 eV at 2 GPa. Their static values $n(0)$ are also listed in Table 4. Our value at 0 GPa is consistent with the values of Ref. [18, 29].

The calculated optical reflectivity $R(\omega)$ at 0, 1 and 2 GPa pressures are displayed in Fig. 5. The calculated reflectivity has maximum values 0.9581, 0.9580 and 0.9582, respectively.
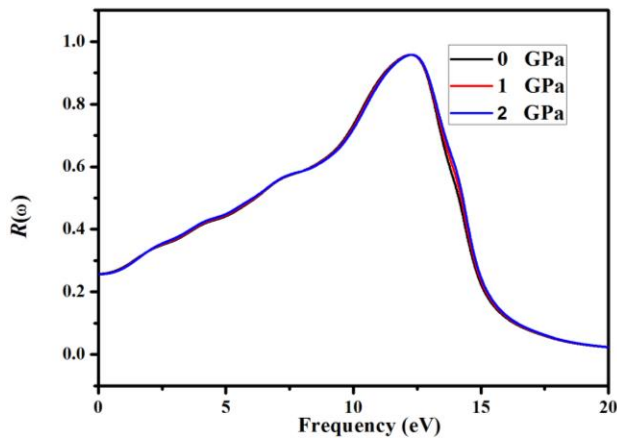
Fig. 5. The Reflectivity R(ω) for AgAlTe₂

3.5. Thermal properties

Through the quasi-harmonic Debye model [30], the thermodynamic properties are obtained from the calculated energy-volume data at 0 K and 0 GPa. Fig. 6 plots relationships between the equilibrium volume V (Bohr^3) and temperatures for various pressures. Meanwhile, V increases slightly as the temperature increases, whereas the equilibrium volume V decreases as the pressure P increases at a given temperature. This account suggests that the AgAlTe₂ under loads turns to be more compressible with increasing pressure than decreasing temperature.
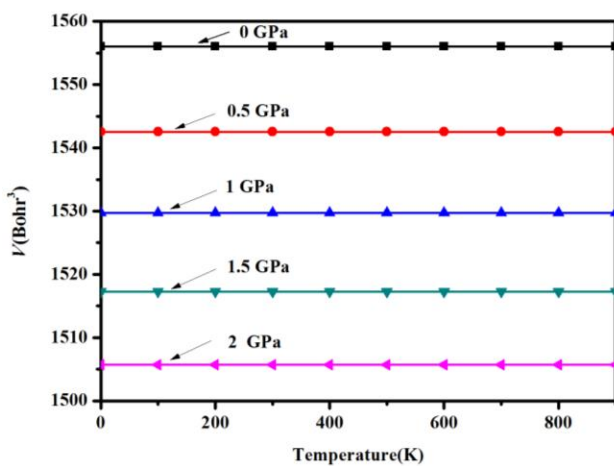
Fig. 6. Volume vs temperature at various pressures for AgAlTe₂
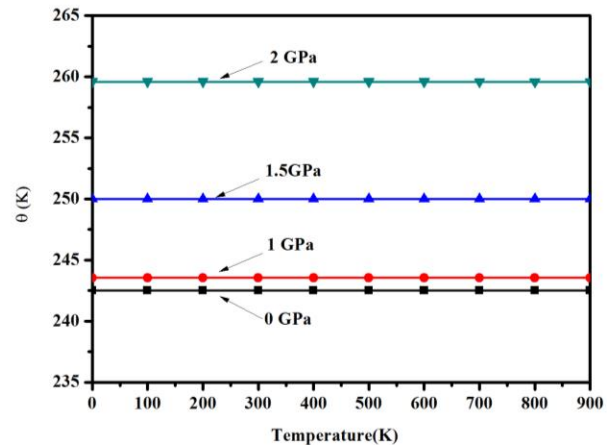
Fig. 7. Debye temperature vs pressure at various temperatures for AgAlTe₂

The variation of the Debye temperature θ (K) as the function of the pressure and temperature are plotted in Fig. 7. With the applied pressure increasing, the Debye temperatures are increasing. At zero pressure and zero temperature, the obtained Debye temperature value is about 232.6 K, which is in good agreement with the value 211.1 K computed accurately in terms of the elastic constants (Table 3). This suggests that the θ obtained from the quasi-harmonic Debye model is quite consistent with that calculated from elastic constants.

Fig. 8 shows the thermal expansion coefficient α (10^{-5}/K) of AgAlTe₂ at various pressures. The thermal expansion coefficient α increases quickly at a given temperature particularly at zero pressure below the temperature of 300 K. After a sharp increase, the thermal expansion coefficient is nearly insensitive to the temperature above 300 K due to the electronic contributions.
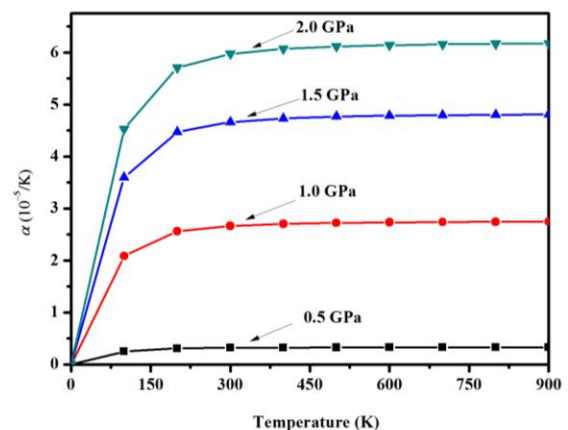
Fig. 8. Thermal expansion coefficient vs pressure at various temperatures for AgAlTe₂

Our calculation of the heat capacities (C_P and C_V) of AgAlTe₂ vs temperature at pressure range 0-15 GPa is shown in Fig. 9. From these figures, we can see that the

constant volume heat capacity C_V and the constant pressure capacity C_P are very similar in appearance and both of them are proportional to T^3 at low temperatures, for higher temperatures the anharmonic approximations of the Debye model is used in which the anharmonic effect on C_V is suppressed and it is very close to the Dulong-Pettit limit, which is common to solids at high temperatures.
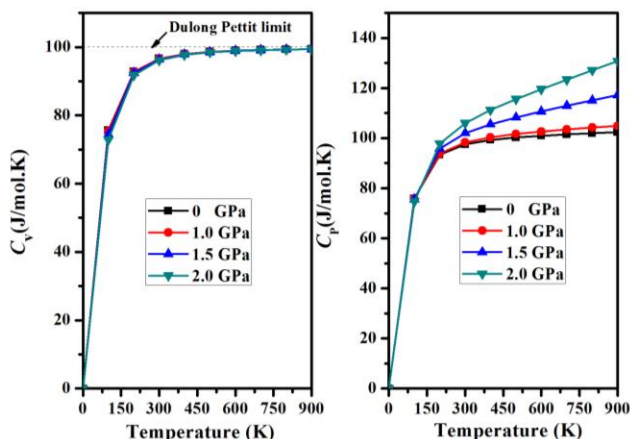
Fig. 9. Heat capacities vs pressure at various temperatures for AgAlTe$_2$

4. Conclusions

The dependences of the structural, elastic and optical properties of AgAlTe$_2$ under pressures were studied using the first-principles method based on the density functional theory with LDA method. The conclusions of this work were drawn specifically as following: The results showed the pressure has the significant impact on the equilibrium optical lattice parameters, mechanical properties, electronic properties of AgAlTe$_2$. The calculated structural and mechanical parameters (bulk modulus B, shear modulus G, Young's modulus E) and Debye temperature θ were in favorable agreement both with the previously reported experimental and theoretical results at zero pressure. The optical properties of the AgAlTe$_2$ have been presented in details. The obtained results are corresponding with other available values. It is hoped that the findings presented may provide data for producing optoelectronic applications. By employing the quasi-harmonic approximation, specific heat, Debye temperature and thermal expansion coefficient are calculated at various temperatures and pressures, and trends are discussed.

References

[1] B. F. Levine, Phys. Rev. B **7**, 2591 (1973).

[2] M. G Panthani, V. Akhavan, B. Goodfellow, J. P. Schmidtke, L. Dunn, A. Dodabalapur, P. F. Barbaba, B. A. Korgel, J. Am. Chem. Soc. **130**, 16770 (2008).

[3] I. Aguilera, J. Vidal, P. Wahnon, L. Reining, S. Botti, Phys. Rev. B **84**, 085145 (2011).

[4] B. Tell, J. L. Shay, H. M. Kasper, Phys. Rev. B **4**, 8 (1971).

[5] J. L. Shay, L. M. Schiavone, E. Buehier, J. H. Wernick, J. Appl. Phys. **43**, 2805 (1972).

[6] K. P. O'Donnell, Semiconductor spectroscopy and device (2014), http://ssd.phys.strath.ac.uk/index.php/

[7] M. Moriya, T. Minegishi, H. Kumagai, M. Katayama, J. Kubota, K Domen, J. Am. Chem. Soc. **135**, 3733 (2013).

[8] J. E. Jaffe, A. Zunger, Phys. Rev. B **29**, 1882 (1984).

[9] W. Honeyman, K. H. Wilkinson, J. Phys. D **4**, 1182 (1971).

[10] S. Mishra, B. Ganguli, Solid State Commun. **151**, 523 (2011).

[11] S. Ullah, H. Ud Din, G. Murtaza, T. Ouahrani, R. Khenata, Naeemullah, S. Bin Omran, J. Alloys Compd. **617**, 575 (2014).

[12] S. Sahina, Y. O. Ciftci, K. Colakoglua, N. Korozlu, J. Alloys Compd. **529**, 1 (2012).

[13] H. J. Hou, H. J. Zhu, J. Xu., S. R. Zhang, L. H. Xie, Braz. J. Phys. **46**, 628 (2016).

[14] D. Vanderbilt, Phys. Rev. B **41**, 7892 (1990).

[15] S. H. Vosko, L. Wilk, M. Nusair, Can. J. Phys. **58**, 1200 (1980).

[16] M. C. Payne, M. P. Teter, D. C. Allen, T. A. Arias, J. D. Joannopoulos, Rev. Mod. Phys. **64**, 1045 (1992).

[17] V. Milan, B. Winker, J. A. White, C. J. Packard, M. C. Payne, E. V. Akhmatskaya, R. H. Nobes, Int. J. Quantum Chem. **77**, 895 (2000).

[18] G M. Dongho Nguimdoa, Daniel P. Joubert, Eur. Phys. J. B **88**, 113 (2015).

[19] J. E. Jaffe, A. Zunger, Phys. Rev. B **29**, 80401 (1983).

[20] H. Hahn, G Frank, W. Klingler, A. D. Meyer, G Střrger, Z Anorg. Allg. Chem. **27**, 1153 (1953).

[21] M. Born, K. Huang, Dynamical Theory of Crystal Lattices (Oxford: Clarendon) (1954).

[22] A. S. Verma, S. Sharma, R. Bhandari, B. K. Sarkar, V. K. Jindal, Mater. Chem. Phys. **132**, 416 (2012).

[23] R. Hill, Proc. Phys. Soc. **65**, 350 (1952).

[24] S. F. Pugh, Philos. Mag. **45**, 833 (1954).

[25] K. B. Panda, K. S. Ravi Chandran, Comput. Mater. Sci. **35**, 134 (2006).

[26] O. L. Anderson, J. Phys. Chem. Solids **24**, 909 (1963).

[27] V. Kumar, A. K. Shrivastava, R. Banerji, D. Dhirhe, Solid State Commun. **149**, 1008 (2009).

[28] P. Y. Yu, M. Cardona, Fundamentals of Semiconductors, Springer-Verlag, Berlin (1996).

[29] P. Mori-Sánchez, A. J. Cohen, W. Yang, Phys. Rev. Lett. **100**, 146401 (2008).

[30] M. A. Blanco, E. Francisco, V. Luana, Comput. Phys. Commun. **158**, 57 (2004).

*Corresponding author: zefer1979@163.com